Journal of Hazardous Materials 418 (2021) 126150

Contents lists available at ScienceDirect

Journal of Hazardous Materials

journal homepage: www.elsevier.com/locate/jhazmat

Research Paper

Delineation of cellular stages and identification of key proteins for reduction and biotransformation of Se(IV) by *Stenotrophomonas bentonitica* BII-R7

M. Pinel-Cabello [a,*], V. Chapon [b], M.A. Ruiz-Fresneda [a,1], B. Alpha-Bazin [c], C. Berthomieu [b], J. Armengaud [c], M.L. Merroun [a]

[a] Department of Microbiology, University of Granada, Campus Fuentenueva s/n, 18071 Granada, Spain
[b] CEA, CNRS, Aix-Marseille Université, BIAM, IPM, 13108 Saint-Paul-lez-Durance, France
[c] Université Paris-Saclay, CEA, INRAE, Département Médicaments et Technologies pour la Santé (DMTS), SPI, 30200 Bagnols sur Cèze, France

ARTICLE INFO

Editor: Dr. R. Debora

Keywords:
Selenium nanostructures
Stenotrophomonas
Microbial Se(IV) reduction
Se(0) biotransformation
Proteomics

ABSTRACT

The widespread use of selenium (Se) in technological applications (e.g., solar cells and electronic devices) has led to an accumulation of this metalloid in the environment to toxic levels. The newly described bacterial strain *Stenotrophomonas bentonitica* BII-R7 has been demonstrated to reduce mobile Se(IV) to Se(0)-nanoparticles (Se(0) NPs) and volatile species. Amorphous Se-nanospheres are reported to aggregate to form crystalline nanostructures and trigonal selenium. We investigated the molecular mechanisms underlying the biotransformation of Se(IV) to less toxic forms using differential shotgun proteomics analysis of *S. bentonitica* BII-R7 grown with or without sodium selenite for three different time-points. Results showed an increase in the abundance of several proteins involved in Se(IV) reduction and stabilization of Se(0)NPs, such as glutathione reductase, in bacteria grown with Se(IV), in addition to many proteins with transport functions, including RND (*resistance-nodulation-division*) systems, possibly facilitating Se uptake. Notably proteins involved in oxidative stress defense (e.g., catalase/peroxidase HPI) were also induced by Se exposure. Electron microscopy analyses confirmed the biotransformation of amorphous nanospheres to trigonal Se. Overall, our results highlight the potential of *S. bentonitica* in reducing the bioavailability of Se, which provides a basis both for the development of bioremediation strategies and the eco-friendly synthesis of biotechnological nanomaterials.

1. Introduction

Selenium (Se) is a fundamental microelement required in trace amounts for many biological processes through its incorporation into selenoproteins, which are involved in myriad physiological functions such as immunity and fertility (Brigelius-Flohé, 2018; Rayman, 2012). Se is widely used in a number of manufacturing industries, including electronics, glass, metallurgy, chemical and pharmaceuticals (Nancharaiah and Lens, 2015; Srivastava and Mukhopadhyay, 2015). However, Se is extremely toxic when exceeding the concentration required for life (Brigelius-Flohé, 2018; Duntas and Benvenga, 2015). Many anthropogenic activities such as mining have increased the environmental flux of Se to reach hazardous levels in water and soils, with the potential to enter the food chain (Etteieb et al., 2020; Zhang et al., 2019). Se is present in low concentrations in the environment in four different oxidation states: selenate [Se(VI)] and selenite [Se(IV)] are the most mobile and toxic species found under oxidizing conditions, whereas elemental Se [Se(0)] and selenide [Se(-II)] are the most common redox states in anoxic environments (Schilling et al., 2020; Winkel et al., 2015). Both Se(0) and Se(-II) species are less water-soluble than Se (VI) and Se(IV), which reduces their bioavailability (Ruiz Fresneda et al., 2018).

Se oxyanions have been shown to be very susceptible to changes in redox state (Schilling et al., 2020). Microorganisms play a key role in the biogeochemical cycle of Se by changing its chemical state, and thus determining its fate and mobility. In this context, Se(IV) reduction has

* Corresponding author.
E-mail address: mariapinel@ugr.es (M. Pinel-Cabello).
[1] Present address: Departamento de Cristalografía y BiologíaEstructural, Instituto de Química-Física Rocasolano (IQFR), CentroSuperior de Investigaciones Científicas (CSIC), Calle Serrano 119, 28006 Madrid, Spain

https://doi.org/10.1016/j.jhazmat.2021.126150
Received 10 February 2021; Received in revised form 30 April 2021; Accepted 14 May 2021
Available online 24 May 2021

been described in bacteria from several different genera, including *Pseudomonas, Rhodococcus* and *Bacillus* (Fischer et al., 2020; Hunter, 2014a; Presentato et al., 2018; Wells et al., 2019), and also fungal species such as *Alternaria alternata* (Rosenfeld et al., 2017).

In recent years, many Gram-positive and -negative bacteria have been investigated for their ability to reduce Se(IV) to immobile and less toxic Se(0), via assimilatory or dissimilatory metabolism or detoxification processes (Nancharaiah and Lens, 2015). Se can be also volatilized in its methylated form (Ruiz-Fresneda et al., 2020). Some of these microorganisms, including *Acinetobacter* sp. SW 30, *Stenotrophomonas maltophilia* SeITE02, *Bacillus subtillis* or *Thauera selenatis,* are able to form intracellular and/or extracellular spherical red-colored Se(0) nanoparticles (SeNPs) (Debieux et al., 2011; Lampis et al., 2017; Wadhwani et al., 2018; Wang et al., 2010) with different physicochemical properties (size, morphology, crystallinity, etc) (Ruiz Fresneda et al., 2018, 2019). The presence of a natural organic coating on biogenic SeNPs (BioSeNPs) of proteins and polymeric substances can also affect their colloidal stability, their interactions with metal ions and their mobility (Fischer et al., 2020).

Microbial-derived SeNPs are typically amorphous (*a*-Se), but the formation of monoclinic and trigonal forms (*m*-Se and *t*-Se, respectively) has also been reported. For example, Srivastava and Mukhopadhyay (2015) described the synthesis of hexagonal-shaped *t*-Se nanorods by *Ralstonia eutropha* cultured with 1.5 mM sodium selenite (Na_2SeO_3) under mesophilic conditions (30 °C). *t*-Se nanostructures have also been produced anaerobically in a thermophilic bioreactor (55 °C) inoculated with anaerobic granular sludge, whereas the BioSeNPs produced in a mesophilic bioreactor (30 °C) were spherical, suggesting the influence of temperature on the process (Dessì et al., 2016). Given the diverse range of applications of SeNPs in different fields, such as cancer therapy or bioremediation of Se-contaminated environments (Gómez-Gómez et al., 2019), the biotechnological synthesis of SeNPs by microorganisms is gaining momentum, in particular nanorods, which have the advantageous characteristics of high settling efficiency and low colloidal stability (Jain et al., 2017). While many studies have suggested different pathways for microbial Se(IV) reduction, including the formation of volatile Se species, little is known about the specific mechanisms involved.

Next-generation proteomics provides valuable information about protein dynamics and cellular processes in complex biological systems (Armengaud, 2016). Differential proteomics based on label-free detection is a robust and proven technology (Gouveia et al., 2020), but only a few studies have applied this to investigate the biochemical pathways and proteins involved in cellular response to Se(IV) exposure in bacteria. For example, Hunter (2014a) identified several enzymes with Se(IV) reductase activity in cell-free extracts of *Pseudomonas seleniipraecipitans,* including glutathione reductase, aspartate-semialdehyde dehydrogenase and isopropylmalate dehydrogenase. A similar study was performed in *S. maltophilia* SeIT02 (Lampis et al., 2017), with a focus on the proteins possibly involved in Se(IV) reduction. Other studies have investigated the proteins that compose the organic layer capping the surface of the SeNPs. Gonzalez-Gil et al. (2016) used proteomics to identify proteins attached to the SeNPs produced by a microbial community of an anaerobic granular sludge from a reactor treating brewery wastewater. They found a large abundance of outer membrane porins and also the elongation factor protein Tu. A similar strategy was used by Fischer et al. (2020) in SeNPs synthesized by *B. safensis* JG-B5T, who detected a variety of proteins from different metabolic pathways including glutathione reductase, thioredoxin reductase and NAD(P)/FAD-dependent oxidoreductases. While informative, these approaches do not give an overall picture of the cellular processes contributing not only to the bioreduction of the metalloid and formation of Se(0) and Se volatile species, but also to mitigate the Se(IV)-related toxicity and, ultimately, the biotransformation of amorphous Se(0) into crystalline Se-containing nanostructures.

The present work focuses on the proteomic and microscopic analysis of Se(IV) bioreduction to Se(0) and SeNPs formation in *Stenotrophomonas bentonitica* BII-R7, a new bacterial strain isolated from bentonite formations in Almería (Spain), which were selected for their use as artificial barriers in a future Spanish nuclear waste repository. We recently reported the transcriptomic response of this biofilm-forming strain to uranium (U) (Pinel-Cabello et al., 2021). Also, *S. bentonitica* BII-R7 shows tolerance to high concentrations of Se(VI) and Se(IV), and can reduce Se oxyanions and produce BioSeNPs under aerobic, anaerobic and alkaline-conditions; specifically, synthesized *a*-Se nanospheres formed *t*-Se nanostructures by aggregation on the extracellular flagella-like structures of the bacterium (Ruiz-Fresneda et al., 2018, 2019). Furthermore, it can further transform Se(0) to volatile Se species (Ruiz-Fresneda et al., 2018, 2020, 2019). In the present study we have applied quantitative proteomics to gain a better understanding of the molecular basis of the interactions of *S. bentonitica* with Se, including the reduction of Se(IV) to Se(0) and the formation of Se volatile species. Our analysis has allowed us to develop a cellular model linking the mechanisms acting synergistically to confer Se(IV) tolerance. We believe that these findings will help in the design of bioremediation technologies for Se(IV)-contaminated environments. Furthermore, the knowledge of these mechanisms might permit the optimization of processes for the biotechnological synthesis of BioSeNPs.

2. Material and methods

2.1. Bacterial culture

S. bentonitica was grown aerobically in Lysogeny broth (LB) medium (tryptone 10 g L^{-1}, yeast extract 5 g L^{-1} and NaCl 10 g L^{-1}, pH 7.0 ± 0.2) at 28 °C with shaking at 150 rpm. After 24 h, cells were washed twice in 0.9% NaCl and inoculated at an initial OD_{600} of 0.2 into LB medium containing 2 mM Na_2SeO_3. Flasks were incubated at 28 °C in a rotatory shaker at 180 rpm. Control treatments without Na_2SeO_3 (biotic) and without bacteria (abiotic) were also established. All treatments were performed with three biological replicates.

Sodium selenite powder (Sigma-Aldrich) was added to Milli-Q water and sterilized by filtration using 0.22 μm filters to prepare a 1 M stock solution.

2.2. Sample preparation and shotgun proteomics

Cells (2–3 mg of wet biomass) were collected at lag, mid-exponential and stationary growth phases (15 min, 14 and 40 h for untreated samples, and 24, 72 and 144 h for treatments with Se(IV)). A total of 18 samples were collected considering each time point, condition and biological replicate. Samples were centrifuged at maximum speed for 10 min. After discarding the supernatants, pellets were immediately frozen in liquid nitrogen and stored at −20 °C until analysis.

Frozen bacterial pellets were suspended in SDS-PAGE loading buffer (100 μL per 1.7 mg of cell pellet for non-treated samples and 100 μL per 3.4 mg of cell pellet for Se(IV)-treated samples, wet weight) containing β-mercaptoethanol. Cell lysis was carried out as described in Hayoun et al. (2019). Experimental procedures for in-gel proteolysis and Nanoscale liquid chromatography coupled to tandem mass spectrometry (NanoLC-MS/MS) are described in detail in the Supplementary Material (S1).

2.3. Mass spectrometry data interpretation

The recorded MS/MS spectra were searched for peptide matches against a database comprising the 3796 annotated proteins from *S. bentonitica* BII-R7 (UniProt database proteome ID UP000175905) (Sánchez-Castro et al., 2017). Peak lists were generated using MASCOT DAEMON software, version 2.5.1 (Matrix Science). Search parameters were set as follows: trypsin as the proteolytic enzyme and a maximum of 2 missed cleavages, 5 ppm mass tolerance for the precursor and 0.02 Da

mass tolerance for the MS/MS signals, fixed modifications for carbamidomethylation of cysteine residues, and glutamine and asparagine deamidation and methionine oxidation as variable modifications. Mascot results were parsed using IRMa software, version 1.31.1c (Dupierris et al., 2009). Peptide-to-spectrum matches were assigned with a *p* value of 0.05, and proteins were validated with the detection of at least two different peptide sequences.

Comparative analysis of protein abundances based on total spectral counts were performed by calculating the T-Fold and *t*-test *p*-values (Excel formula, Microsoft) previously developed for the PatternLab software (Carvalho et al., 2008), and following standard normalization. The proteins were classified according to their T-Fold and *p*-values. Only proteins with T-Fold $\geq$1.5 or $\leq$−1.5 and with a *p*-value $\leq$0.05 (defined here as the "Blue class") were retained. The estimated detection of the spectral counts and their abundances were visualized by grouping them into a hierarchical cluster tree using the R package pvclust (n = 2000 bootstrap), utilizing the war.D method and spearman distance, to establish the similarity/dissimilarity between the samples. The Pearson correlation coefficient was calculated using the R package reshape2. Proteins that passed a cut-off of −0.9 and 0.9 were used to build an interaction network in Cytoscape, version 3.8.2 using the Betweenness Centrality of each node.

MS proteomics data have been deposited in the ProteomeXchange Consortium via the PRIDE partner repository (Perez-Riverol et al., 2019) with the dataset identifier PXD023459 and project DOI 10.6019/PXD023459.

2.4. HAADF-STEM and EDX spectrometry analyses

To determine the cellular localization and to characterize the physicochemical properties (size, morphology and structure) of the SeNPs produced by the cells as a consequence of Se(IV) reduction, cells were harvested at the different growth phases for microscopic analyses. Samples of 1 mL of Se(IV)-treated cell cultures were taken after 24, 72 and 144 h of incubation and centrifuged at 11,000 rpm for 10 min at room temperature. Cell pellets were fixed in 0.1 M cacodylate buffer (pH 7.2) with 2.5% glutaraldehyde during 24 h at 4 °C. Cells were then washed with the same cacodylate buffer and stored at 4 °C until sample preparation, as described in Merroun et al. (2005). Samples were analyzed using high-angle annular dark field scanning transmission electron microscopy (HAADF-STEM) on a FEI TITAN G2 80–300 microscope with an energy dispersive X-ray (EDX) spectrometer. Selected-area electron diffraction (SAED) and high resolution TEM (HRTEM) combined with fast Fourier transform (FFT) enabled the structure characterization of the nanostructures. TEM specimen holders were cleaned with plasma prior to analysis to avoid contamination.

3. Results

3.1. Growth of S. bentonitica in the presence of Se(IV)

Growth of *S. bentonitica* BII-R7 was evident with or without the addition of 2 mM Na_2SeO_3. Se(IV) reduction was revealed by the appearance of a red color in the culture after 24 h of incubation (Fig. 1), which became more intense at longer incubation periods, denoting an increase in the amount of reduced Se(IV). As expected, no color change was observed in the abiotic control, indicating that Se(IV) reduction was mediated by *S. bentonitica* (Fig. 1). It has been previously reported that *S. bentonitica* BII-R7 exhibits a 48-h lag phase in the presence of 2 mM Se (IV), and that the stationary growth phase is reached at ~100 h (Ruiz-Fresneda et al., 2018 and Fig. S1). Accordingly, we sampled the cultures for proteomic analysis at 24, 72 and 144 h, to cover all the growth phases.

3.2. General overview of shotgun proteomics

The nanoLC-MS/MS analysis of the 18 samples yielded 1,151,245 MS/MS recorded spectra, of which 682,785 could be assigned to peptide sequences of *S. bentonitica* BII-R7 proteome with a *p*-value $\leq$0.05. The high assignment rate (60%) indicated good quality MS/MS spectra. The spectra were assigned to 12,150 unique peptide sequences, which represented 1922 proteins validated by at least two independent peptides matches. The entire experimental dataset corresponded to ~50% of the predicted proteome of the strain. Hierarchical clustering analysis was used to determine the similarity of the inter-sample protein profiles. Se (IV)-treated and untreated samples grouped into two different clusters, which in turn could be divided into three subgroups corresponding to each growth phase (Fig. S2). The uniformity between replicate samples indicated the high reproducibility of the experimental procedure. Analysis of the protein pools obtained for the untreated and Se(IV)-treated samples at each growth phase revealed that the majority of proteins were common to the three growth phases (around 86% of the proteome), irrespective of the treatment (Fig. S3). Indeed, only ~10% of the detected proteins were specific to the Se(IV)-treated or non-treated cells at each growth phase, although the total number of proteins detected was lower in Se(IV)-treated samples than in untreated samples.

Considering the proteins classified in the Blue class (proteins identified with a fold change $\geq$1.5 or $\leq$−1.5 and *p*-value $\leq$0.05), a total of 828 proteins were detected with significant differences in abundance between Se(IV)-treated and non-treated samples: 271 in lag phase, 458 in exponential phase and 505 in stationary phase (Fig. 2). A total of 511 proteins were differentially abundant for a particular growth phase and 89 proteins were common between the three growth phases, of which 38 were significantly more abundant in Se(IV)-treated samples and 43 proteins were significantly more abundant in non-treated samples

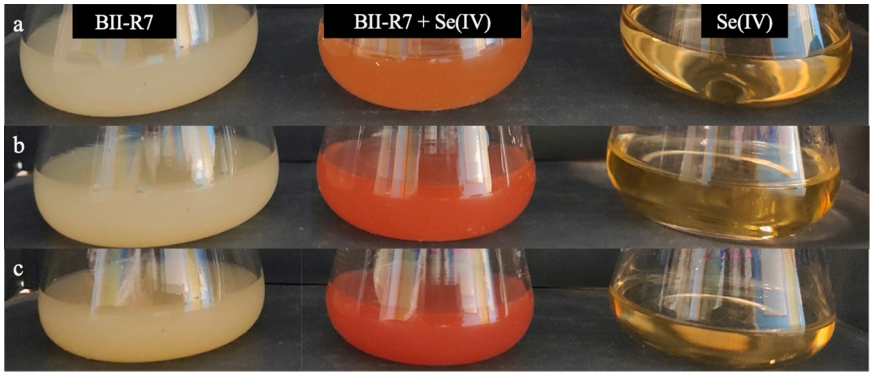

Fig. 1. Color change of *Stenotrophomonas bentonitica* BII-R7 cultures supplemented with 2 mM Se(IV) at 24 (a), 48 (b) and 72 h (c) of incubation. No color changes were detected in biotic and abiotic control cultures.

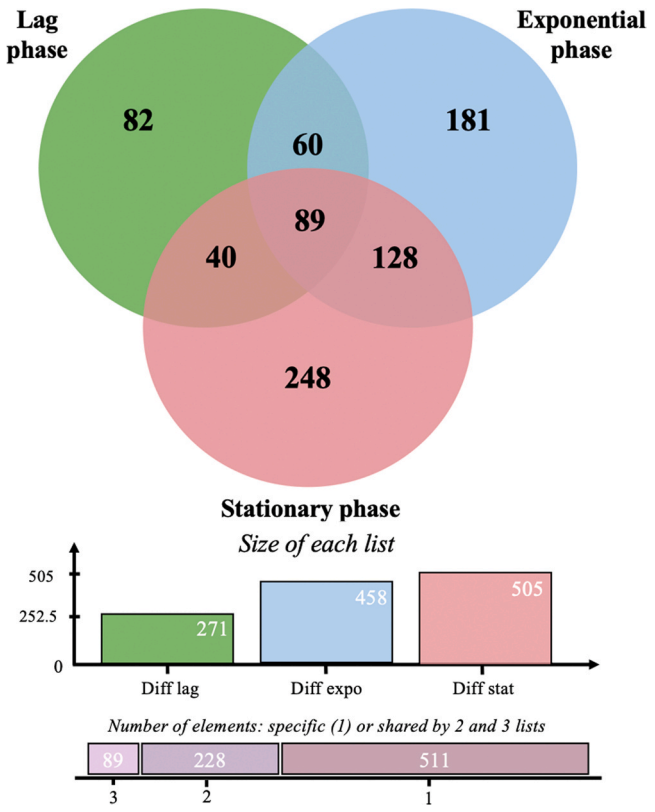

Fig. 2. Venn diagram comparing Blue class proteins at lag (green), exponential (blue) and stationary (red) growth phases. (For interpretation of the references to color in this figure legend, the reader is referred to the web version of this article.)

(Fig. 2). We built an interaction network based on the positive and negative correlations between the 89 common proteins (represented as P1 to P89) (Fig. 3), highlighting the complex response triggered by Se (IV). The correspondence between the numbers on the figure and the proteins is indicated in Supplementary Table S1. Among the proteins establishing the highest number of interactions were 2 hypothetical proteins (P72, P81), a sulfurtransferase (P15), the chemotaxis protein CheW (P52), an FMN-dependent NADH-azoreductase (P12), a glutathione peroxidase (P54) and a diguanylate cyclase (P74). Only the sulfurtransferase and the FMN-dependent NADH-azoreductase were more abundant in Se(IV)-treated cells than in non-treated cells, particularly during the stationary phase (6- and 14.7-fold change, respectively). Of note, the FMN-dependent NADH-azoreductase correlated positively with many enzymes implicated in oxidative stress, such as catalase/peroxidase HPI, which was highly abundant in the stationary phase. The remaining aforementioned proteins were less abundant in Se(IV)-treated than in untreated cells, with the lowest fold changes found during the exponential phase: -3-, -7.5-fold change for the hypothetical proteins P72 and P81, -5-fold change for diguanylate cyclase, and -2.3- and -4.5-fold changes for CheW and glutathione peroxidase, respectively.

3.3. Proteome response over time in S. bentonitica during Se(IV) stress

The 828 proteins whose abundance was significantly altered by Se (IV) were related to a variety of metabolic pathways, and could be classified into 6 groups according to their predicted function: oxidoreductases, transporters, participants in stress response, transcriptional regulators, general metabolism and motility. Ninety-six of the 828 proteins were classified as hypothetical proteins due to the lack of their functional characterization. Of the 89 common proteins with significant changes detected in all growth phases, the abundance of several was specifically altered at a given culture time.

Approximately 24% of the 89 common proteins of different metabolic processes were annotated as oxidoreductase proteins (Table 1). Although evident along the entire experiment, the greatest number of oxidoreductases was found in the stationary phase, where they were generally more abundant than in the other growth phases. Also, oxidoreductase proteins were generally more abundant in Se(IV)-treated than in untreated samples. The oxidoreductase showing the greatest fold change was FabG protein, an NAD/NADP-dependent 3-oxoacyl-ACP reductase belonging to the short-chain dehydrogenase/reductase (SDR) family, which showed a fold change of 76.5 during the lag phase in Se(IV)-treated cells. A dioxygenase showed the second greatest change in abundance, with a 27.3-fold change in the lag phase. Both FabG and the dioxygenase followed the same tendency of a progressive decrease in the fold change in the exponential and stationary phases (14.1 and 11.7-fold changes for FabG; 15.3 and 12.7-fold changes for dioxygenase, respectively). In addition, the subunit F of an alkyl hydroperoxide reductase showed the most significant fold change of this group during stationary growth. The subunit C of the alkyl hydroperoxide reductase was also more abundant in Se(IV)-treated than in untreated samples albeit to a lesser extent (Table 1). This latter oxidoreductase exhibited the opposite behavior to the other two aforementioned enzymes, with an increase in its fold change along time, especially between the exponential and stationary phases for the subunit F (from 6.5- to 33.4-fold change). Furthermore, ArsH and ArsC, two reductases involved in arsenic resistance with NADPH-dependent FMN reductase and arsenate reductase activity, respectively, were more abundant in the presence of Se(IV) in the lag (4.3 and 2.4-fold change, respectively) and stationary (10 and 7.8-fold change, respectively) phases. Also worthy of note was the finding of an increased abundance of enzymes involved in glutathione metabolism such as glutamate—cysteine ligase, glutathione synthase and glutathione-disulfide reductase, in Se(IV)-treated cells (Table 1). The fold change of glutamate—cysteine ligase increased over time, while glutathione synthase fold change increased in the lag phase. Other enzymes including an SDR family aklaviketone reductase, malate:quinone oxidoreductase and glutaredoxin 3 (GrxC family) also increased in abundance over time. Nevertheless, some proteins in this category decreased in abundance with Se(IV) exposure, particularly the alpha subunit of a ribonucleoside-diphosphate reductase, with fold change values from −4.1 to −33.7 in the lag to stationary phase. Furthermore, a cyclic pyranopterin phosphate synthase involved in the synthesis of the Mo cofactor (MoCF), needed for the activity of oxidoreductases in carbon, nitrogen and sulfur metabolism, had the lowest fold change values in the lag phase, and further decreased during the exponential growth phase (from −12.3 to −17.7).

Of the 89 proteins shared in the three growth phases, nine were involved in stress response in Se(IV)-treated cells, including proteins implicated in DNA modification and repair, chaperones, cold- and heat-shock proteins and enzymes that provide protection against reactive oxygen species (ROS). One of these proteins, a catalase/peroxidase HPI, showed a notable increase in abundance over time, especially from the exponential (20.5-fold change) to the stationary (257-fold change) phase. Indeed, this protein was not only the most up-regulated in abundance in this growth phase, but also in the entire experiment. Of note, proteins involved in stress response exhibited an increase along the culture time, suggesting their importance during the stationary phase, since more proteins related to this process showed positive fold changes at this sampling time. During the lag phase, the stress response was represented mostly by proteins involved in DNA repair (e.g., RadA, recombinase RmuC, RecA), enzymes tasked with protecting cells from oxidative stress (e.g., catalase/peroxidase HPI, organic hydroperoxide resistance), and the ATP-dependent chaperone ClpB. The number of chaperone proteins showing greater abundance increased at the exponential and stationary phases, such as DnaK, HtpG and GroEL, with higher fold changes at the latter growth phase (2.4-, 1.8- and 2.3-fold for

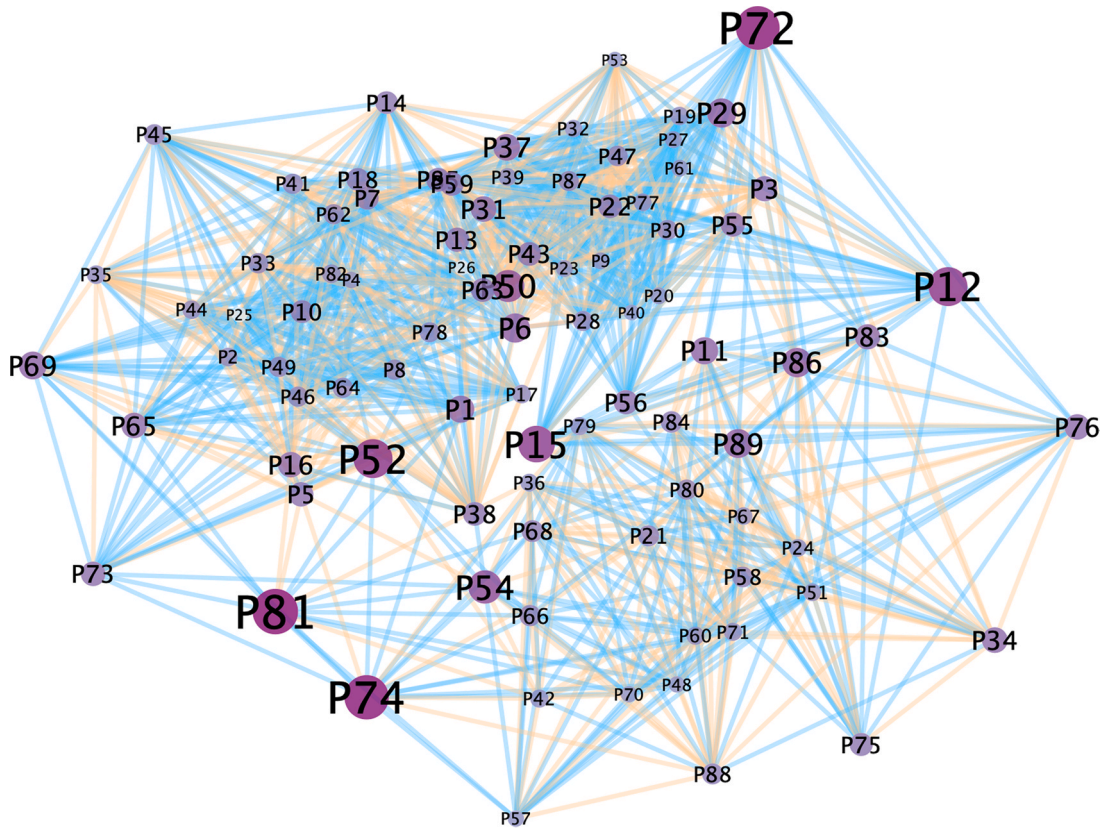

Fig. 3. Network of positive (blue) and negative (red) interactions between Blue class proteins found in all growth phases tested. The size of the nodes is proportional to the number of interactions of each protein. (For interpretation of the references to color in this figure legend, the reader is referred to the web version of this article.)

DnaK, HtpG and GroEL, respectively), including ClpB (from 1.8 in the exponential growth to 3.5-fold change in the stationary phase).

Of the proteins involved in regulatory mechanisms, a heavy metal-responsive transcriptional regulator was more abundant only in the stationary phase (3-fold change). Two YhaK-family proteins, previously related to biofilm formation in *Escherichia coli* (Hancock et al., 2010) also increased in abundance in Se(IV)-treated cells, one of them during the exponential phase (25-fold change). In line with this, a UDP-N-acetylenolpyruvoylglucosamine reductase (MurB) and the monofunctional biosynthetic peptidoglycan transglycosylase (MtgA), both involved in peptidoglycan biosynthesis, increased in abundance in the stationary and lag phases, respectively (3.8- and 1.5-fold changes). The RelE protein from the toxin/antitoxin system RelE/RelB, increased in abundance during the lag (2-fold change) and exponential (3.3-fold change) phases.

Approximately 9% of the 89 common proteins of the Blue class had a predicted transporter function, such as TonB-dependent or metal transporters, with RND-type efflux systems being the most significantly abundant in the lag and exponential phases. The permease subunit of an AcrB multidrug efflux RND transporter was 81-fold more abundant in Se(IV)-exposed cultures than in untreated cultures after 24 h, and remained high along the culture time (39- and 49-fold changes during exponential and stationary phases, respectively). Similar results were observed for another RND transporter, a lipoprotein of the NodT family (43- and 46-fold changes in lag and exponential phases, respectively), which decreased in abundance to nearly 50% once *S. bentonitica* entered stationary growth (21-fold change). Moreover, a probable CircA TonB-dependent receptor and the permease subunit SmeE from RND family were exclusively produced during exponential growth. Specific transporters in the stationary phase included an AcrB subunit from a multidrug pump and a copper-transporting ATPase. However, nitrogen and iron uptake systems were negatively affected by Se(IV), as illustrated by the decreased abundance of Fis, Fur and FecR transcriptional regulators.

Analysis of the specific changes in abundance during the lag phase showed that many proteins belonging to ribosomal subunits were increased (ranging from 6.3- to 1.5-fold changes), whereas very few were detected in the following hours. Proteins of general metabolism, such as the subunit 3 of gluconate 2-dehydrogenase family protein (−8.8-fold change in the exponential phase), were found to be mainly lower in abundance than in non-treated samples in all growth phases. However, a greater number of proteins involved in cell division (*e.g.*, FtsX, FtsZ or FtsK), elongation factors, DNA polymerases and helicases (*e.g.*, DEAD/DEAH box helicase), as well as amino acid, carbohydrate and lipid metabolism proteins (*e.g.*, sugar hydrolase), were detected in Se(IV)-treated cells in the exponential and stationary phases. Finally, very few proteins related to motility processes (*e.g.*, PilT and CheW) were found in the Blue class, and all were less abundant than in the non-treated samples.

3.4. Microscopic characterization of Se(IV) bioreduction using HAADF-STEM and EDX

We performed HAADF-STEM analysis to determine the cellular localization and structural properties of the bioreduction products of Se (IV). Micrographs of samples at 24 h (lag phase) revealed the presence of only a few electron-dense Se-containing nanospheres inside cells (Fig. 4). The SAED pattern clearly indicated their amorphous nature (Fig. 4c). Both intra- and extracellular Se-nanospheres were more evident after 72 h (exponential phase), with an increased size ranging from 120 to 350 nm (Fig. 5). Finally, only a few nanospheres, mainly present in the extracellular space, were found after 144 h of incubation (stationary phase). Notably, at this time/phase we could observe that

Table 1
Differentially abundant proteins with oxidoreductase activity present in all growth phases.

Protein description	TFold (Se-treated vs non-treated samples)		
	Lag phase	Exponential phase	Stationary phase
Short-chain dehydrogenase	76.50	14.10	11.69
Dioxygenase	27.33	15.33	12.67
NADPH:quinone reductase	10.00	6.00	2.00
NAD(P)H dehydrogenase	10.00	8.00	6.67
FMN-dependent NADH-azoreductase	6.67	4.67	14.67
3-beta hydroxysteroid dehydrogenase	6.64	5.43	3.14
Malonic semialdehyde reductase	4.97	3.51	2.56
Luciferase-like monooxygenases	3.08	6.71	9.13
Alkene reductase	2.96	5.56	12.40
Glutathione synthase	2.13	1.70	1.76
Oxidoreductase	1.98	2.05	2.87
Alkyl hydroperoxide reductase subunit F	1.84	6.51	33.38
Oxidoreductase	1.83	2.42	4.50
Alkyl hydroperoxide reductase subunit C	1.76	2.39	3.90
Glutathione-disulfide reductase	1.73	2.09	1.54
Alkene reductase	1.72	2.62	2.69
Fe-S cluster assembly ATPase SufC	1.71	1.81	1.72
Fe-S cluster assembly protein SufD	1.69	2.38	3.58
Thioredoxin-disulfide reductase	1.53	2.11	1.68
Aldehyde dehydrogenase iron-sulfur subunit	-1.62	-4.42	-1.75
FAD-dependent monooxygenase	-1.74	-2.03	-11.33
Glutathione peroxidase	-1.75	-4.50	-2.27
Molybdopterin dehydrogenase	-1.95	-5.22	-2.22
Oxidoreductase	-2.00	-4.50	-1.89
Molybdopterin converting factor subunit 2 protein	-2.00	-2.60	-4.67
Twin-arginine translocation pathway signal	-2.67	-8.75	-3.00
GMC family oxidoreductase	-3.05	-5.70	-2.14
Coproporphyrinogen III oxidase	-6.50	-4.50	-12.33

some nanospheres were located next to damaged or lysed cells (Fig. 6).

Samples incubated for 72 and 144 h were characterized mainly by the presence large Se nanostructures in the extracellular space, which also contained sulfur (S) in their structure as indicated by the EDX analysis (Fig. 8c). Irregular Se nanostructures were also observed at these sampling times (Fig. 5c, d, e), which seemed to be formed by the aggregation of Se-nanospheres. Irregular aggregations found at 144 h differed from those observed in 72 h by the presence of small gaps in their structure (Fig. 6c). Patterns obtained from SAED analysis revealed the amorphous nature of the nanostructures (Fig. 5f). However, crystalline structures such as nanowires were also found at both incubation times (Figs. 7a, d and 8). HRTEM analyses along with the FFT of the nanowires formed after 72 h indicated two lattice spacings of 0.2 and 0.32 nm, which would correspond to different planes (1 2 5; −2 4 1) and (1 1 3) of *m*-Se, respectively (Fig. 7b and c). Lattice spacings measured in samples collected at 144 h were 0.3, 0.37 and 0.49 nm, which could correspond to different planes of both *m*-Se and *t*-Se (Fig. 7e and f). Specifically, the D-spacing of 0.3 nm could correspond to planes (1 0 1) of *t*-Se and (2 2 1) of *m*-Se. The D-spacing of 0.37 nm clearly corresponded to the plane (1 0 0) of *t*-Se. Finally, the lattice spacing of 0.49 nm is close to that found at 0.45 nm, which could be related to the plane (0 2 0) of *m*-Se.

Elemental mapping of both irregular and crystalline nanostructures observed at 72 and 144 h of incubation showed S in their structure, in contrast to nanospheres at 24 h where no S was detected, probably due to their small size (Fig. 9).

4. Discussion

4.1. General overview of proteomics data

Comparative proteomics analysis of *S. bentonitica* BII-R7 cultured with or without Se(IV) showed that the majority of proteins were less abundant in the Se(IV)-treated samples than in the controls, particularly during the exponential and stationary phases. These results are in line with the findings of Ruiz-Fresneda et al. (2018), who observed that *S. bentonitica* BII-R7 growth was highly affected by the presence of the metalloid, with an extended lag phase and a lower final cell density as compared with non-treated samples. The lower percentage of total proteins detected during the lag phase in Se(IV)-treated samples than in untreated samples is consistent with previous observations (Ruiz-Fresneda et al., 2018, 2020), and the negative effect of Se(IV) on bacterial growth is supported by the increased expression of the RelE protein of the RelE/RelB toxin-antitoxin system, which promotes growth arrest in this phase (Kolodkin-Gal et al., 2009). The number of total proteins detected in Se(IV)-treated samples was slightly higher in the lag phase than in the exponential phase. Despite the lack of growth in this phase, *S. bentonitica* was metabolically active, likely to counteract the toxicity of the oxyanion and reduce the amount of soluble Se(IV). According to the results of Ruiz-Fresneda et al. (2020), the duration of the lag phase of *S. bentonitica* is equivalent irrespective of the initial concentration of Se(IV), suggesting that cells adapt to the toxicity of the toxic oxyanion rather than recovering growth when a certain amount of Se(IV) is reduced.

4.2. Proteins involved in Se(IV) transport into the cells

Microscopy analysis of Se(IV)-treated *S. bentonitica* revealed the intracellular reduction of Se(IV) to Se(0) and subsequent formation of Se (0) nanospheres. There is a paucity of information in the literature about how Se(IV) can reach the cytoplasm. Our proteomic analysis points to the involvement of outer membrane transporters like the RND lipoprotein NodT, TonB-dependent transporters, metal transporters or porins in this process. The RND lipoprotein NodT is best known for its role as a transporter of small molecules such as antibiotics and toxic compounds across the two cell envelopes (Ibrahim et al., 2012). Another outer membrane protein with a probable function in Se(IV) uptake is the TonB-dependent receptor CircA (3.08- and 3.29-fold changes in lag and exponential phase). That being said, the energy transducer TonB protein that interacts with the TonB-dependent receptor to perform the transport function across the outer membrane (Noinaj et al., 2010) was reduced in abundance in Se(IV)-treated cells at all incubation periods, suggesting a different role for the receptor, perhaps signaling environmental information. Other metal cation transporters including a dicarboxylate/amino acid:cation symporter and the magnesium transporter MgtE (found 4- and 1.6-fold higher in lag phase, respectively) were also detected. A phosphate selective porin OprP was up-regulated in the lag and exponential phases (1.8- and 2.1-fold change, respectively). In line with our findings, Gonzalez-Gil et al. (2016) proposed that Se(IV) could reach the periplasm through outer membrane porins, and the porin-like protein ExtI along with ExtH has been recently related to Se(IV) uptake in *Geobacter sulfurreducens* (Jahan et al., 2019), suggesting a possible role of OprP in Se(IV) transport. The greater abundance of proteins of other transport systems like AcrAB, SmeE or CcmA, widely known to provide antibiotic resistance (Hayashi et al., 2015; Marquez, 2005), might point to their role in maintaining the integrity of the cell envelope, which could be disturbed by the oxyanion (Huang et al., 2014). Changes in the abundance of proteins including lipocalin Blc, during the lag phase, and the down-regulation of the cell shape determination bactofilin CcmA, also suggest envelope stress (Campanacci et al., 2006; Taylor et al., 2020). This hypothesis is supported by the microscopy observations, showing the detachment of the plasma membrane from the cell wall in some cells, as also reported by Poirier et al. (2016) in

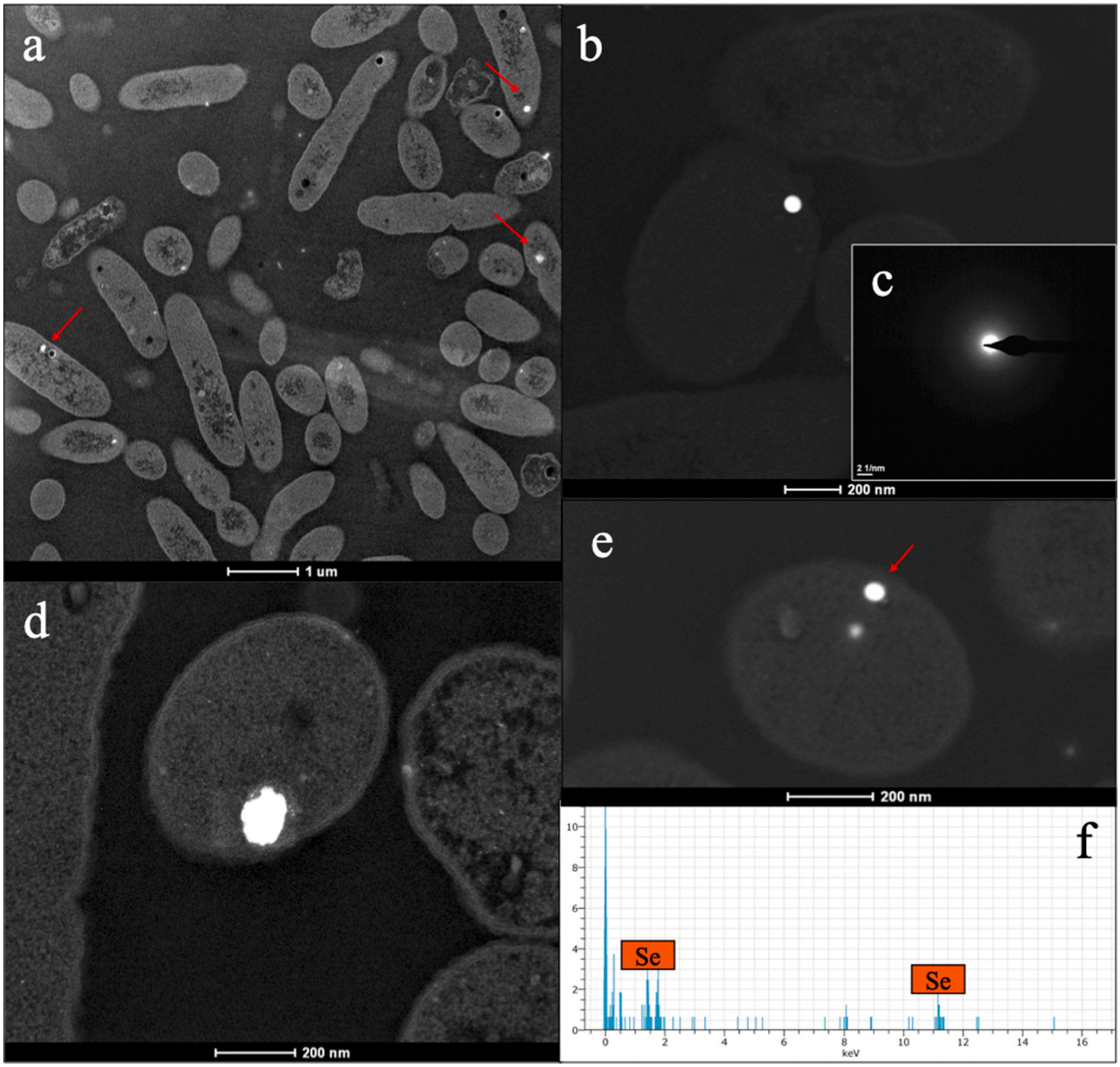

Fig. 4. HAADF-STEM micrographs of amorphous nanospheres formed by *Stenotrophomonas bentonitica* BII-R7 cultured with 2 mM Se(IV) after 24 h of incubation (a, b, d, e). EDX analysis (f) of a nanosphere (e) revealing Se in its composition.

Pseudomonas fluorescens BA35SM1 exposed to CdSe NPs. Exposure of *S. bentonitica* to U triggered a similar response, with an increase in transcription of AcrAB, SmeED and the TonB-dependent receptor as a consequence of the interaction of the radionuclide with the cell (Pinel-Cabello et al., 2021).

4.3. Proteins implicated in bioreduction of Se(IV) and formation of Se(0) NPs and Se volatiles species

It has been previously demonstrated that *S. bentonitica* can reduce Se (IV) to elemental SeNPs intracellularly during the first 24 h, which appeared extracellularly at 72–144 h (Ruiz-Fresneda et al., 2018). The abundance of enzymes such as glutathione synthase, glutathione-disulfide reductase and thioredoxin-disulfide reductase was increased in Se(IV)-treated cells, suggesting their role in the reduction of this metalloid. Proteobacteria possess abundant thiol-containing compounds, and several studies have described the contribution of glutathione (GSH), glutaredoxin or thioredoxin in Se(IV) bioreduction (Fischer et al., 2020; Khoei et al., 2017; Nancharaiah and Lens, 2015). Indeed, Antonioli et al. (2007) reported the key role of GSH in *S. maltophilia* SeITE02 in the early stages of a Se(IV) response (lag and exponential phases) and highlighted the importance of the glutathione reductase in maintaining the pool of reduced GSH. This is in line with our results, which also found differences in these systems between growth phases in *S. bentonitica*. During the lag phase, the cell uses the existing pool of reduced GSH and glutaredoxin for Se(IV) bioreduction in the first place, and begin synthesizing new GSH molecules from glutamate, cysteine and/or glycine via the glutamate—cysteine ligase and glutathione synthase (1.5- and 2.1-fold change, respectively). During exponential growth, *S. bentonitica* replenishes GSH via glutathione-disulfide reductase (2.1-fold change). It is also worth noting the up-regulation of enzymes that produce NADPH, a cofactor needed

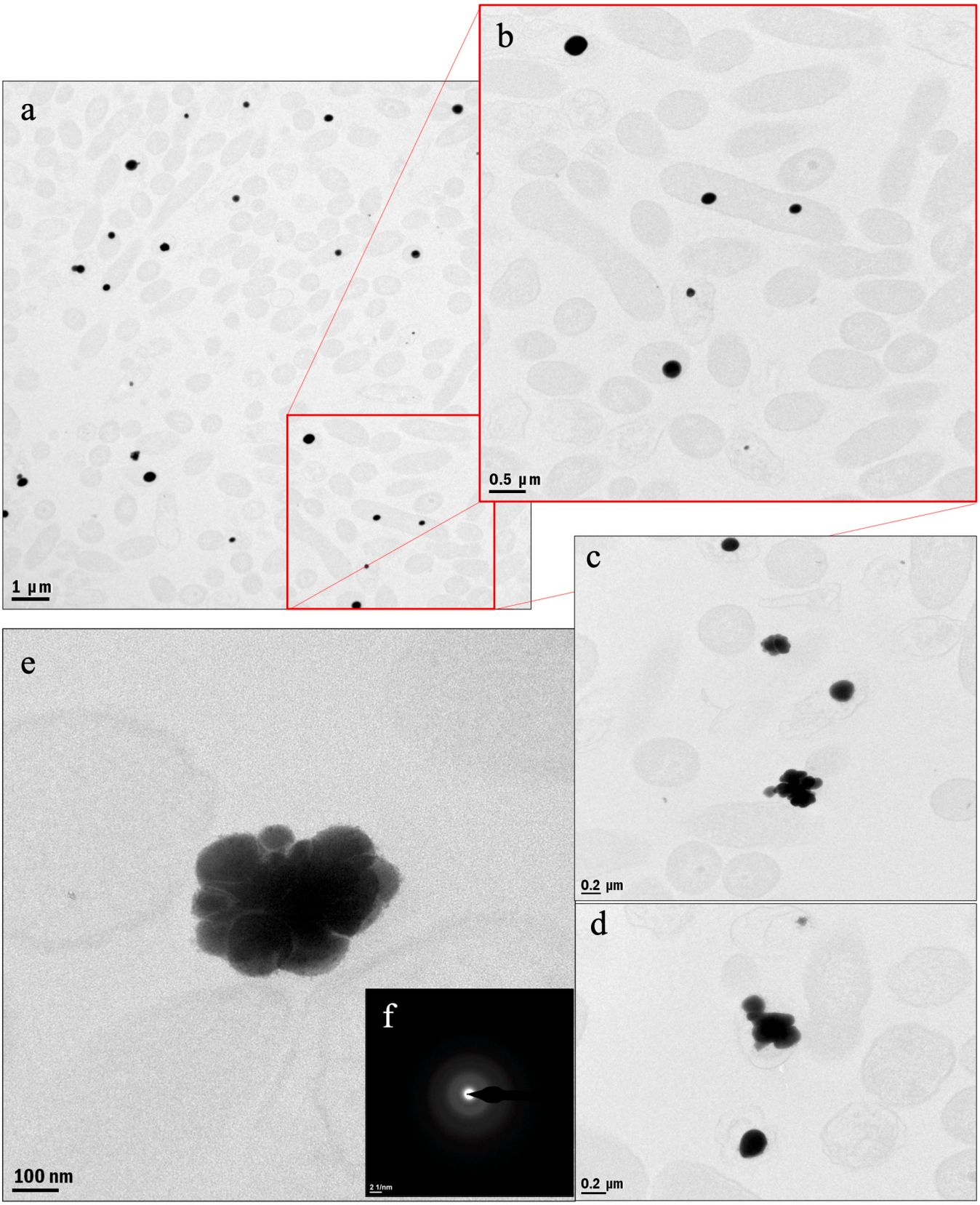

Fig. 5. Micrographs of selenium nanoparticles (a, b) and irregular structures (e, c, d) formed after 72 h of incubation. SAED patterns revealing its amorphous nature (f).

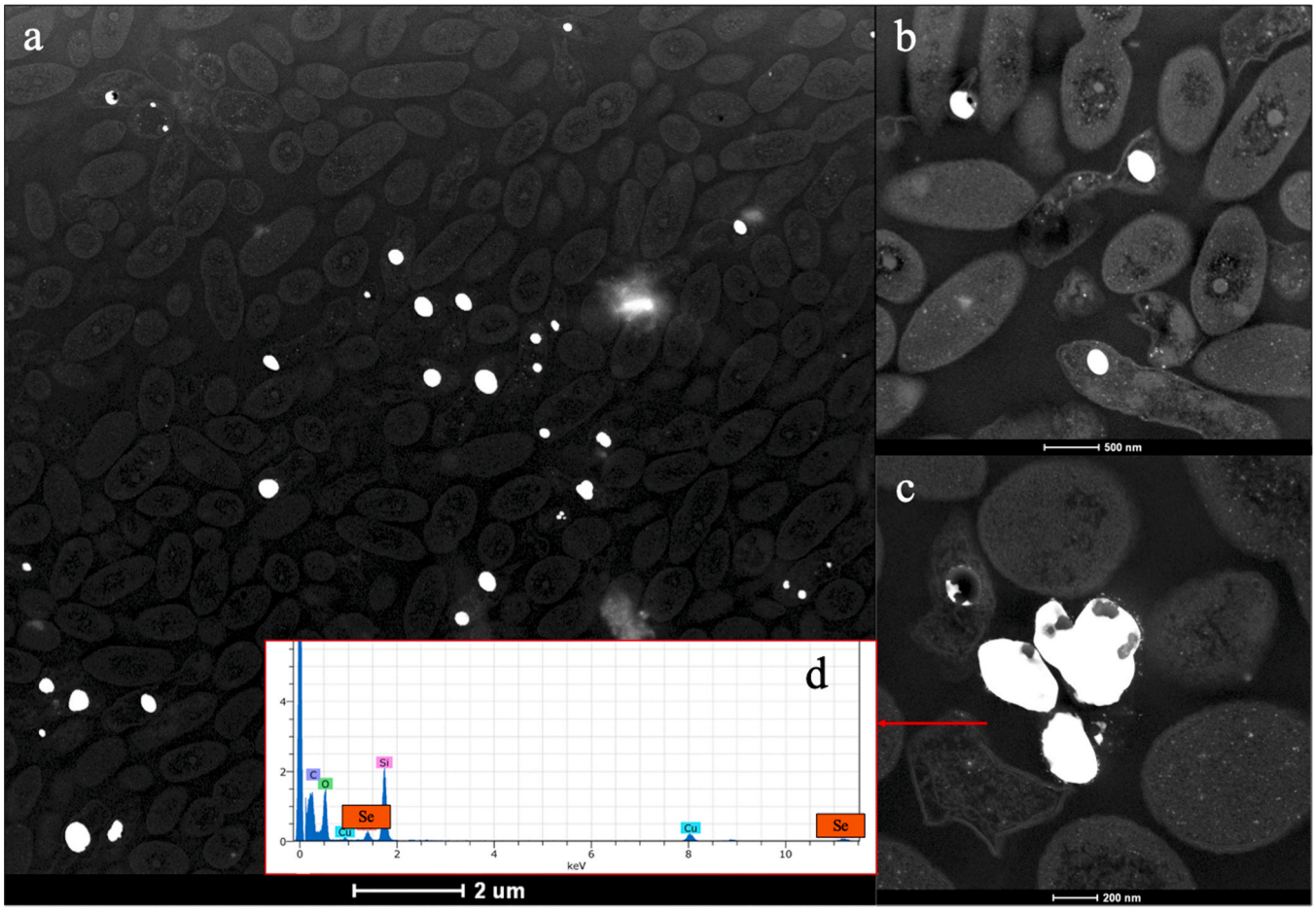

Fig. 6. Selenium nanospheres (a, b) and irregular aggregation (c) from *Stenotrophomonas bentonitica* BII-R7 after 144 h culture with 2 mM Se(IV). EDX analysis showed the presence of selenium in the irregular aggregations (d).

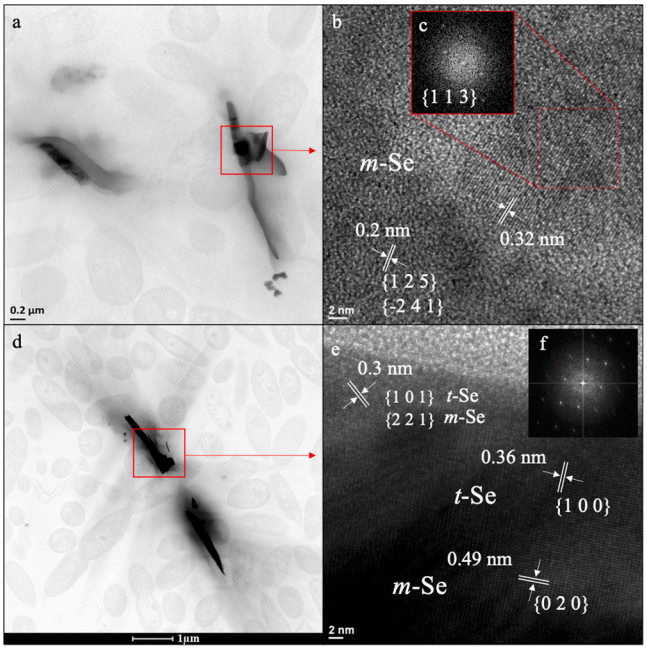

Fig. 7. *Stenotrophomonas bentonitica* BII-R7 containing selenium nanowires. Micrographs and HRTEM with FTT analysis from 72 h (a, b and c) and 144 h of incubation (d, e and f).

for the reduction of oxidised glutathione, such as 6-phosphogluconate dehydrogenase (1.6- and 1.5-fold change in exponential and stationary growth phases) from the pentose phosphate pathway, during exponential and stationary phases. Thioredoxin-disulfide reductase showed a similar behavior to glutathione-disulfide reductase, suggesting that thioredoxin is also implicated in Se(IV) bioreduction.

Other mechanisms for Se(IV) reduction are likely to occur simultaneously. Enzymes such as 3-oxoacyl-ACP reductase (FabG), dioxygenase, or NADPH:quinone reductase, were highly induced during the lag phase (76.5-, 27.3- and 10-fold change, respectively). FabG, a family member of SDR, was previously detected in *Pseudomonas moraviensis* subsp. stanleyae, with Se(IV) reductase activity in the presence of NADPH (Filip'echeva et al., 2018; Ni et al., 2015). Similarly, NAD(P)H reductases have been previously related to Se(IV) reduction in some bacteria, including *Burkholderia fungorum* strain 95 (Khoei et al., 2017). Proteins from the old yellow enzyme family such as alkene reductase could be involved in Se(IV) reduction to Se(0) and protection against oxidative stress (Hunter, 2014b). ArsC from the *ars* operon, which reduces arsenate in presence of thioredoxin, GSH or glutaredoxin, might also perform Se(IV) reduction (2.4- and 7.8-fold changes in lag and stationary phases, respectively). While the majority of the induced oxidoreductases in *S. bentonitica* were cytoplasmic, the finding of some periplasmic enzymes suggests that bioreduction can also occur in this cellular compartment. Bioreduction of Se(IV) in the periplasm has been previously demonstrated in other bacteria such as *Shewanella oneidensis* MR-1 via fumarate reductase (Li et al., 2014).

Some proteins may also play a role in the formation and stabilization of BioSeNPs, by controlling their size. An example of this is alcohol

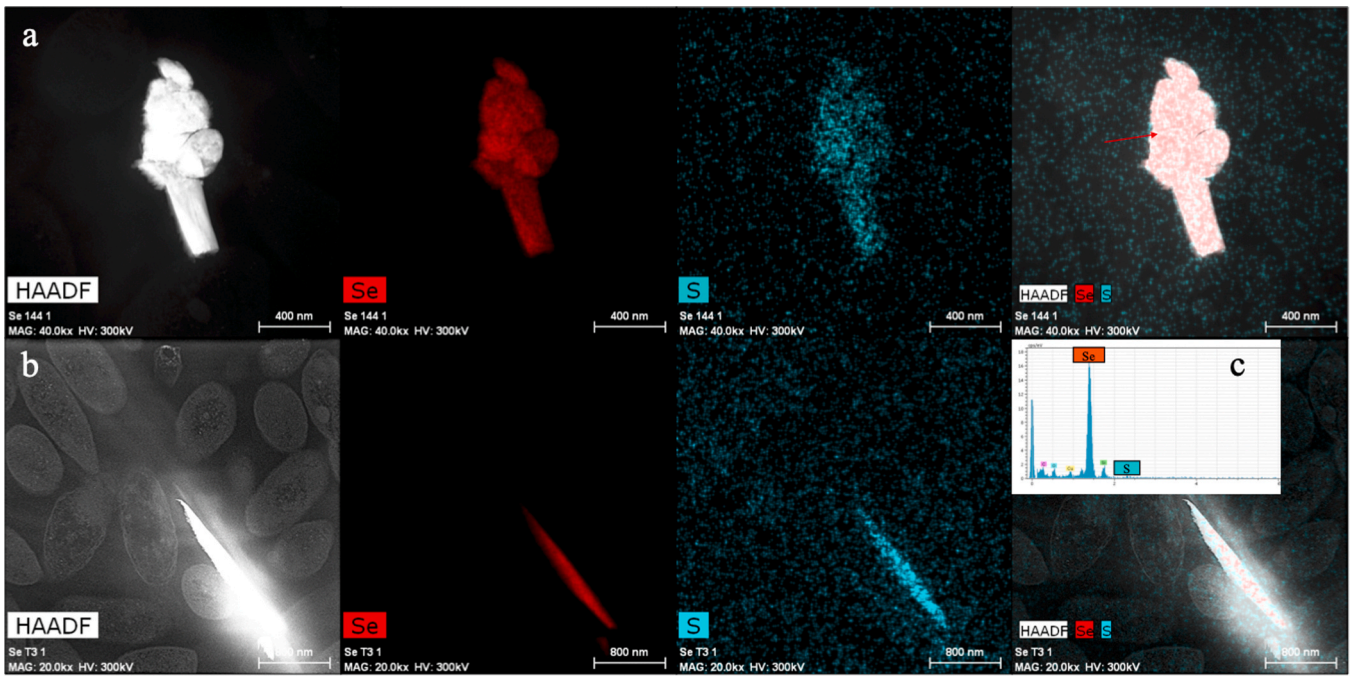

Fig. 8. Elemental mapping of crystalline aggregation and nanowires observed in *Stenotrophomonas bentonitica* BII-R7 at 144 h of incubation. Nanostructures are mainly composed of selenium and sulfur.

dehydrogenase, which has been previously found attached to SeNPs produced by *E. coli*, and is also found in *S. maltophilia* SeITE02 and *P. seleniipraecipitans* in the presence of Se(IV) (Dobias et al., 2011; Hunter, 2014a; Lampis et al., 2017). Up-regulation of proteins for Fe-S cluster assembly were also identified in the present study, including members of the Suf system. Fischer et al. (2020) reported on different proteins of this system attached to the surface of SeNPs produced by *Bacillus safensis* JG-B5T, suggesting their role in reduction and stabilization of the SeNPs. A possible implication of Fe-S cluster assembly proteins in oxidative stress response has also been previously suggested, such as SufC in *Lactobacillus reuteri* CRL 1101 (Gómez-Gómez et al., 2019; Poirier et al., 2016). Ni et al. (2015) proposed glutathione reductase as one of the main enzymes involved in nanoparticle formation in *P. moraviensis*, and suggested a probable function in stabilization and size control of the nanospheres. The hypothesis of bioreduction and stabilization of SeNPs mediated by thiol groups in *S. bentonitica* is supported by the accumulation of sulfur in Se nanostructures, suggesting that GSH metabolism is implicated in the biotransformation of Se nanospheres to different nanostructures.

Overall, our findings suggest that reduction in *S. bentonitica* occurs by several different mechanisms that act synergistically along the culture period. Ruiz-Fresneda et al. (2020) studied the reduction rate of Se(IV) in this strain under the same conditions. They reported that 100% Se(IV) reduction is reached after 120 h of incubation. However, Se(IV) bioreduction in *S. bentonitica* might not be limited to Se(0)NP formation, and these authors demonstrated the further reduction of Se(0) to volatile methylated forms including dimethyl diselenide (DMDSe) and dimethyl selenyl disulfide (DMSeDS) (Ruiz-Fresneda et al., 2020). Formation of volatile Se species have been observed in other bacteria, and even fungi (Eswayah et al., 2019, 2016; Kessi, 2006). The mechanisms involve reduction and methylation reactions, and intermediaries including dimethyl selenone or methyl selenol have been detected (Eswayah et al., 2019; Harrison et al., 1984). Kessi (2006) reported that inhibition of glutathione synthesis in *Rhodospirillum rubrum* and *Rhodobacter capsulatus* reduced the formation of methylated Se, suggesting that thiol groups are also involved in reduction of the Se oxyanion to selenide. Thioredoxin reductase catalyzes two steps of selenocompound metabolism: the transformation of selenite to hydrogen selenide and methyl selenic acid to methyl selenol. We found that thioredoxin reductase increased in abundance along all growth phases in *S. bentonitica*, possibly participating in the formation of the volatile reduced forms of Se. Methyltransferases are likely involved in the transfer of methyl groups, such as thiopurine methyltransferase from *P. syringae*, which uses S-adenosylmethionine as a methyl group donor (Ranjard et al., 2002). Accordingly, methyltransferases methylate hydrogen selenide and methyl selenol to form dimethyl-selenide. Methyltransferases were increased in abundance in Se(IV) treated *S. bentonitica* at all time points including some S-adenosylmethionine-dependent enzymes such as class I rRNA methyltransferase in the stationary phase (2-fold change). These findings suggest that thiols and methyltransferases likely constitute a pathway for Se-methylation in *S. bentonitica.* Biomethylated selenium is less toxic than other species of the metalloid, offering an efficient mechanism for long-term elimination of Se oxyanions in soil and water (Eswayah et al., 2016).

4.4. Proteins involved in ROS and stress protection

A consequence of the high reductase activity to counter Se(IV) toxicity in *S. bentonitica* is an increase in oxidative stress (Gómez-Gómez et al., 2019). This likely explains the increase of proteins involved in ROS and stress protection, such as catalases, DNA repair proteins, chaperones and proteases. For example, the thiol:disulfide interchange protein DsbG, a disulfide isomerase that corrects non-native disulfide bonds and prevent aggregation of misfolded proteins (Collet and Bardwell, 2002), was increased in the lag phase (1.7-fold change) over non-treated cells, which might indicate protein damage in the periplasm as a consequence of the entrance of the oxyanion. It is important to highlight the massive induction of the catalase/peroxidase HPI observed at 144 h (257-fold change), which has increased effectiveness under high doses of H_2O_2 (Poirier et al., 2016). The catalase HPII was also detected in the stationary phase albeit to a lesser extent (2-fold change). The tremendous over-production of catalase/peroxidase HPI once Se (IV) reduction is complete suggests the involvement of this protein in other processes. Further studies are needed to elucidate the role of this enzyme during stationary phase. Oxidoreductases such as luciferase-like monooxygenase, alkyl hydroperoxide reductase subunit F and C might

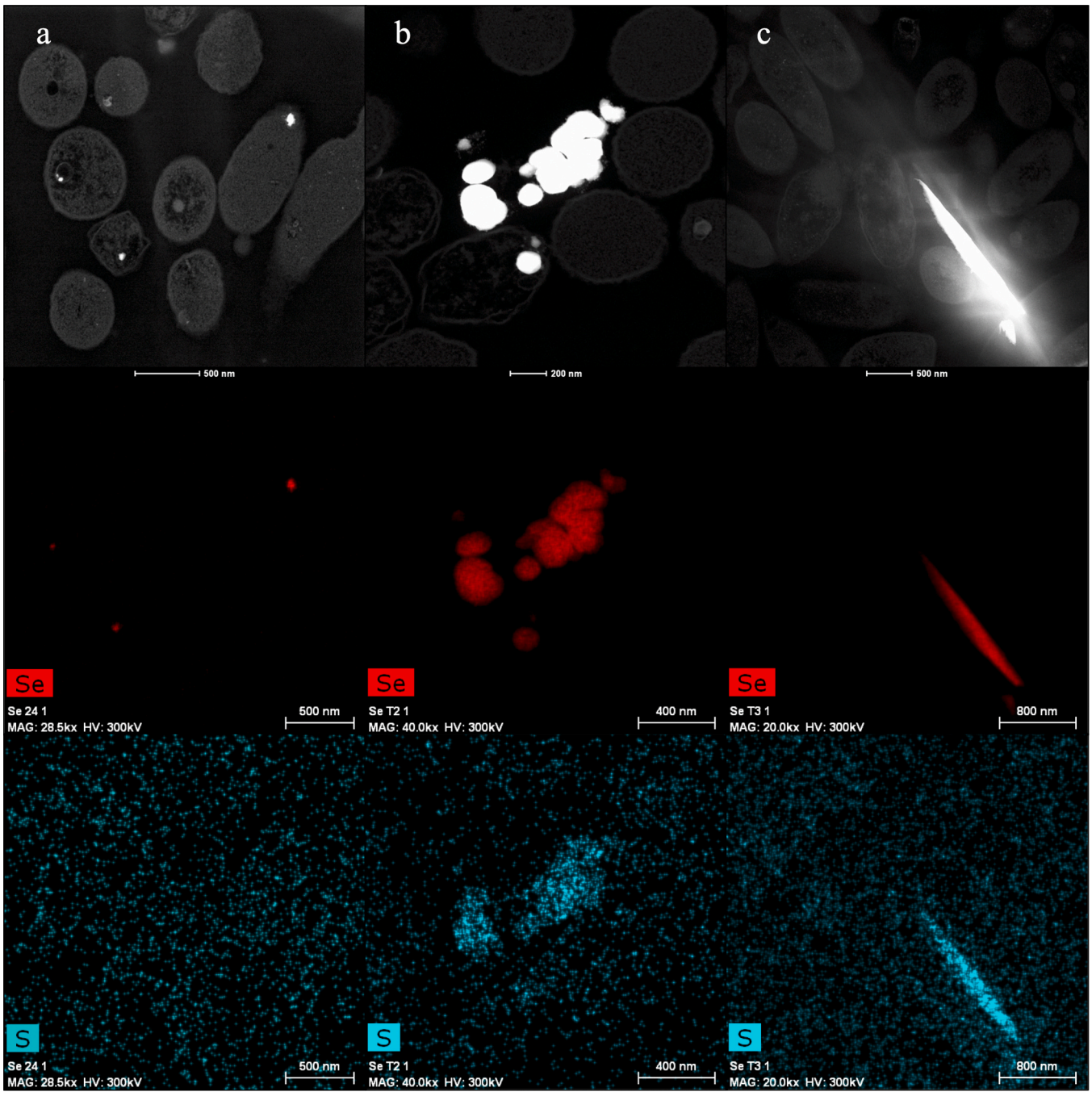

Fig. 9. Biotransformation process from *a*-nanospheres (a, 24 h), to an intermediate stage of amorphous aggregations (b, 72 h), which ultimately form crystalline structures (c, 144 h).

also have a role in mitigating oxidative stress (Poirier et al., 2016). Studies have demonstrated that ArsH, from the *ars* operon, can protect from oxidative damage (Hervás et al., 2012; Vorontsov et al., 2007). The fold change of this enzyme increased progressively along the time course, concomitantly with oxidative stress in the cells due to the Se(IV) reduction, which support this hypothesis.

4.5. Biotransformation of amorphous (a)-Se to trigonal (t)-Se nanostructures

Production of *a*-Se nanospheres by *S. bentonitica*, and their subsequent biotransformation to crystalline Se nanostructures, was confirmed by HAADF-STEM analyses. STEM micrographs revealed the presence of intracellular *a*-Se nanospheres at early incubation periods appearing progressively in the extracellular medium along the time course, in line with previous observations by Ruiz-Fresneda et al. (2018) using the same strain. The ability to reduce Se(IV) to Se(0) has been reported in many phylogenetically-diverse microorganisms (Nancharaia and Lens, 2015). Wang et al. (2018) reported the biosynthesis of extracellular SeNPs in *Proteus mirabilis* YC801, and Ni et al. (2015) reported intracellular SeNPs in *P. moraviensis* subsp. stanleyae. *S. oneidensis* MR-1 also produced intracellular SeNPs under anaerobic conditions (Li et al., 2014). Several mechanisms have been suggested to explain how SeNPs are exported outside the cell (Debieux et al., 2011; Nancharaiah and Lens, 2015). Some authors propose the formation of vesicles as a stress response to release SeNPs (McBroom and Kuehn, 2007), whereas others

suggest cellular lysis or specific transporters such as Selenium factor A (SefA) described in *Thauera selenatis* (Debieux et al., 2011). As lysed cells were found near to some extracellular nanospheres and no vesicles were observed in the STEM micrographs, we would hazard that cellular lysis is likely the mechanism explaining the release of SeNPs in *S. bentonitica*. This hypothesis is supported by the higher induction of the toxin RelE during the exponential phase.

Once in the extracellular milieu, *a*-Se nanospheres transform to trigonal Se with different sizes and morphologies (polygons, nanowires, etc.). The amorphous aggregations found at 72 h of incubation suggests an intermediate form before transformation to the observed *m*-Se and *t*-Se nanostructures, in agreement with results of Ruiz-Fresneda et al. (2018, 2020, 2019). In these studies, *m*-Se was suggested as a possible intermediary crystalline structure produced by *S. bentonitica*. However, the presence of *m*-Se in such nanostructures is demonstrated here for the first time, confirming the transformation process from *a*-Se to *m*-Se, and finally to *t*-Se, which is the most thermodynamically stable form of Se.

It has been proposed that SeNPs can act as seeds in a nucleation mechanism, allowing an increase in size following a process similar to Ostwald ripening (Lampis et al., 2017; Nancharaiah and Lens, 2015). Other authors have described the importance of organic capping compounds associated with the nanospheres in this process (Bao et al., 2016; Debieux et al., 2011; Xu et al., 2018). It is known that SeNPs synthesized by *S. bentonitica* are coated with an amine-rich organic layer (Ruiz--Fresneda et al., 2020). Fischer et al. (2020) identified the proteins coating SeNPs formed by *B. safensis* JG-B5T, with many corresponding to those detected here in *S. bentonitica* BII-R7 such as thioredoxin-disulfide reductase, glutathione reductase, SufC, D and B, or alcohol dehydrogenase. Following Se(IV) reduction, these enzymes could bind SeNPs to stabilize them and allow aggregation to form nanostructures, explaining the accumulation of S in the nanostructures by the adhesion of GSH or Suf system proteins, among others. Nevertheless, it is also possible that these proteins adhere to the SeNPs during cellular lysis (Fischer et al., 2020). Further studies are needed to determine the role of specific proteins in the biotransformation process of a-Se nanospheres to *t*-Se.

4.6. Cellular mechanism of Se(IV) detoxification in S. bentonitica

The next-generation label-free shotgun proteomics and microscopic observations in the present work allowed us to develop a cellular model of biotransformation of Se(IV) in *S. bentonitica* (Fig. 10). *S. bentonitica* exposed to Se(IV) adapts to the toxicity during the 48 h lag phase. The process begins with Se(IV) uptake, possibly mediated by proteins like RND systems, porins or other metal transporters, across the envelopes. The oxyanion could also bind to the cell wall, causing envelope disruption, which would lead to activation of mechanisms to maintain membrane homeostasis (lipocalin Blc, SmeE, AcrAB or CcmA) (Campanacci et al., 2006; Huang et al., 2014). Once inside the cell, Se(IV) would damage the structure of proteins, inducing the activity of chaperones or proteases to prevent the accumulation of misfolded proteins. The bacteria would also utilize oxidoreductase enzymes from different pathways to reduce Se(IV) to Se(0), with the subsequent production of SeNPs. Proteins involved in thiol metabolism, particularly GSH synthesis (glutathione-disulfide reductase, glutamate—cysteine ligase, glutathione synthase, etc.), 3-oxoacyl-ACP reductase FabG from fatty acid synthesis, or NAD(P)H-reductases, are some of the proposed cytoplasmic enzymes (Khoei et al., 2017; Nancharaiah and Lens, 2015; Ni et al., 2015). The nature of these mechanisms in the first 48 h allows the strain to counteract Se(IV) toxicity, and the exponential phase of growth begins. Bioreduction would also lead to the formation of volatile DMDSe and DMSeDS by the activity of thioredoxin reductase and methyltransferases (Eswayah et al., 2016; Ruiz-Fresneda et al., 2020).

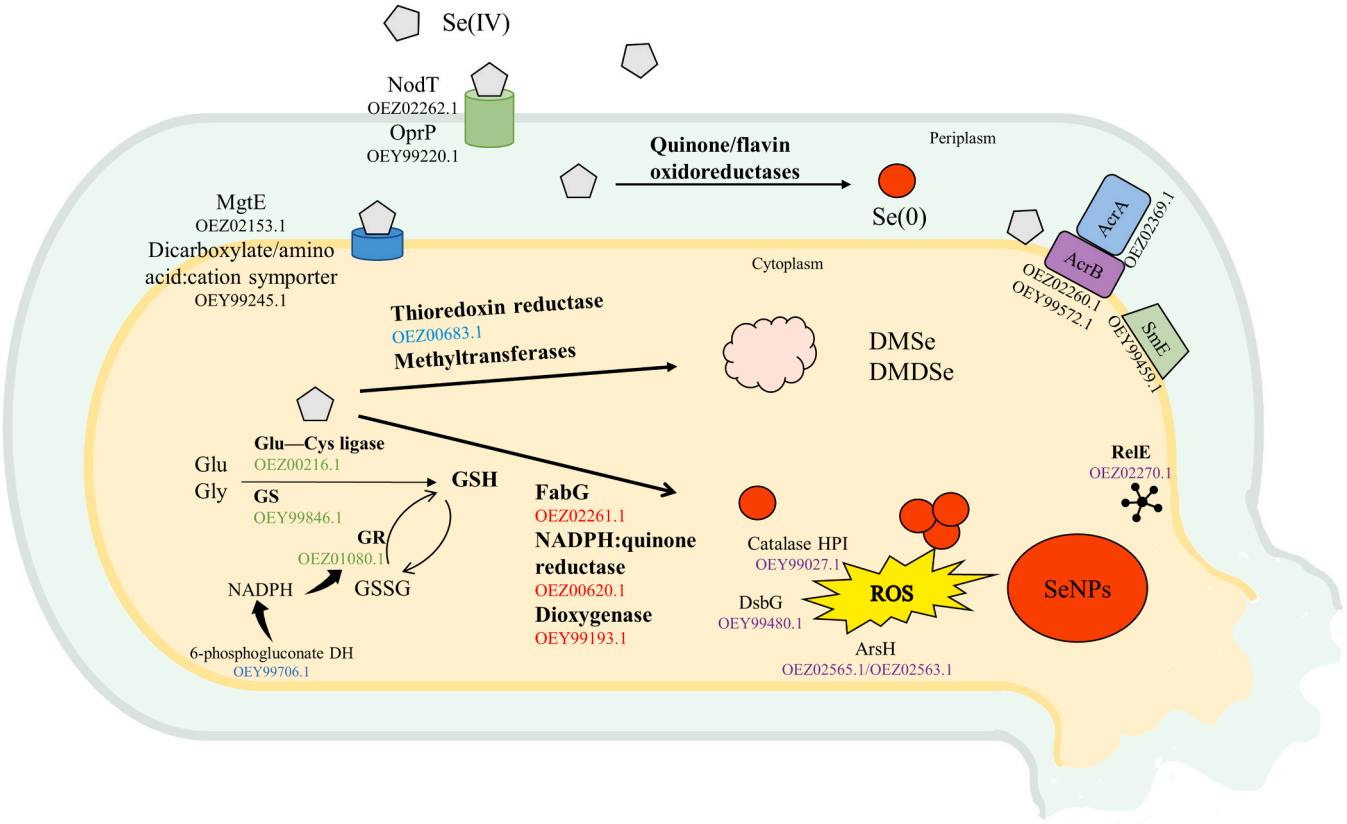

Fig. 10. Cellular mechanism of Se(IV) tolerance in *Stenotrophomonas bentonitica* BII-R7. Se(IV) is transported inside the cell, where it can be reduced until the formation of selenium nanoparticles or to volatile species (DMSe and DMDSe). The selenium nanoparticles would expand in the cytoplasm until their release into the extracellular milieu by cell lysis.

Subsequently, intracellular nanospheres would increase in size as more Se(IV) is reduced, resulting in increased oxidative stress and ROS production, in turn inducing proteins for DNA repair (DnaA, RadA, recombinases RmuC and RecA, etc.), chaperones (e.g., ClpB), and catalases, such as catalase/peroxidase HPI (Poirier et al., 2016). The stress caused by the metalloid itself and the greater size of the BioSeNPs would induce proteins related to cell death such as toxin RelE (Kolodkin-Gal et al., 2009), leading to the release of the nanospheres to the extracellular medium. During cellular lysis, different proteins would attach to the surface of SeNPs, forming the observed coating material (Fischer et al., 2020). This organic layer would trigger the coalescence of the *a*-nanospheres until the formation of amorphous and irregular aggregations, which would transform into crystalline structures of *m*-Se, and ultimately into *t*-Se.

Our findings indicate that *S. bentonitica* can efficiently biotransform toxic Se(IV) into a stable immobile form, reducing its bioavailability. The label-free shotgun proteomic approach described here provides high-quality molecular-specific data not only about proteins and enzymes implicated in the Se(IV) reduction process, but also on the probable metabolic pathways that act against Se(IV) toxicity, giving a full overview of the response of *S. bentonitica* to the oxyanion and providing a starting point to prioritize specific targets for further analysis Understanding the behavior of the enzymes and biomolecules implicated in this process is of great importance for the development of bioremediation strategies, and also for the eco-friendly and cost-effective synthesis of nanomaterials for important technological applications, such as in the electronic and biomedical industries.

CRediT authorship contribution statement

M. Pinel-Cabello: Conceptualization, Methodology, Investigation, Formal analysis, Visualization, Writing - original draft, Funding acquisition. **V. Chapon:** Conceptualization, Supervision, Methodology, Investigation, Resources, Writing - review & editing. **M.A. Ruiz-Fresneda:** Conceptualization, Writing - review & editing. **B. Alpha-bazin:** Methodology, Investigation, Formal analysis, Resources, Writing - review & editing. **C. Berthomieu:** Resources, Writing - review & editing. **J. Armengaud:** Methodology, Resources, Formal analysis, Writing - review & editing. **M.L. Merroun:** Conceptualization, Supervision, Methodology, Resources, Writing - original draft, Funding acquisition.

Declaration of Competing Interest

The authors declare that they have no known competing financial interests or personal relationships that could have appeared to influence the work reported in this paper.

Acknowledgements

This work was supported by the grants obtained by M.P-C: (FPU 15/04284; “Formación de Profesorado Universitario”) and EST 18/00610 (“Ayudas a la movilidad para estancias breves y traslados temporales”) from Spanish Ministry (Ministerio de Universidades). Funding was also provided by grants CGL2014-59616-R; RTI2018.101548.B.I00 to M.L. M. Funding for open access charge: University of Granada / CBUA. The authors thank Concepción Hernández-Castillo and María del Mar Abad Ortega for their assistance with microscopy at the University of Granada (“Centro de Instrumentación Científica”). We also thank Dr. Kenneth McCreath for editorial support.

Appendix A. Supporting information

Supplementary data associated with this article can be found in the online version at doi:10.1016/j.jhazmat.2021.126150.

References

Antonioli, P., Lampis, S., Chesini, I., Vallini, G., Rinalducci, S., Zolla, L., Righetti, P.G., 2007. *Stenotrophomonas maltophilia* SeITE02, a new bacterial strain suitable for bioremediation of selenite-contaminated environmental matrices. Appl. Environ. Microbiol. 73, 6854–6863. https://doi.org/10.1128/AEM.00957-07.

Armengaud, J., 2016. Next-generation proteomics faces new challenges in environmental biotechnology. Curr. Opin. Biotechnol. 38, 174–182. https://doi.org/10.1016/j.copbio.2016.02.025.

Bao, P., Xiao, K.Q., Wang, H.J., Xu, H., Xu, P.P., Jia, Y., Häggblom, M.M., Zhu, Y.-G., 2016. Characterization and potential applications of a selenium nanoparticle producing and nitrate reducing bacterium *Bacillus oryziterrae* sp. nov. Sci. Rep. 6 https://doi.org/10.1038/srep34054.

Brigelius-Flohé, R., 2018. Selenium in human health and disease: an overview. In: Michalke, B. (Ed.), Selenium, Molecular and Integrative Toxicology. Springer International Publishing, Cham, pp. 3–26. https://doi.org/10.1007/978-3-319-95390-8_1.

Campanacci, V., Bishop, R.E., Blangy, S., Tegoni, M., Cambillau, C., 2006. The membrane bound bacterial lipocalin Blc is a functional dimer with binding preference for lysophospholipids. FEBS Lett. 580, 4877–4883. https://doi.org/10.1016/j.febslet.2006.07.086.

Carvalho, P.C., Hewel, J., Barbosa, V.C., Yates III, J.R., 2008. Identifying differences in protein expression levels by spectral counting and feature selection. Genet. Mol. Res. 7, 342–356. https://doi.org/10.4238/vol7-2gmr426.

Collet, J.-F., Bardwell, J.C.A., 2002. Oxidative protein folding in bacteria: oxidative protein folding in bacteria. Mol. Microbiol. 44, 1–8. https://doi.org/10.1046/j.1365-2958.2002.02851.x.

Debieux, C.M., Dridge, E.J., Mueller, C.M., Splatt, P., Paszkiewicz, K., Knight, I., Florance, H., Love, J., Titball, R.W., Lewis, R.J., Richardson, D.J., Butler, C.S., 2011. A bacterial process for selenium nanosphere assembly. Proc. Natl. Acad. Sci. USA 108, 13480–13485. https://doi.org/10.1073/pnas.1105959108.

Dessì, P., Jain, R., Singh, S., Seder-Colomina, M., van Hullebusch, E.D., Rene, E.R., Ahammad, S.Z., Carucci, A., Lens, P.N.L., 2016. Effect of temperature on selenium removal from wastewater by UASB reactors. Water Res. 94, 146–154. https://doi.org/10.1016/j.watres.2016.02.007.

Dobias, J., Suvorova, E.I., Bernier-Latmani, R., 2011. Role of proteins in controlling selenium nanoparticle size. Nanotechnology 22, 195605. https://doi.org/10.1088/0957-4484/22/19/195605.

Duntas, L.H., Benvenga, S., 2015. Selenium: an element for life. Endocrine 48, 756–775. https://doi.org/10.1007/s12020-014-0477-6.

Dupierris, V., Masselon, C., Court, M., Kieffer-Jaquinod, S., Bruley, C., 2009. A toolbox for validation of mass spectrometry peptides identification and generation of database: IRMa. Bioinformatics 25, 1980–1981. https://doi.org/10.1093/bioinformatics/btp301.

Eswayah, A.S., Hondow, N., Scheinost, A.C., Merroun, M., Romero-González, M., Smith, T.J., Gardiner, P.H.E., 2019. Methyl selenol as a precursor in selenite reduction to Se/S species by methane-oxidizing bacteria. Appl. Environ. Microbiol. 85, e01379-19 https://doi.org/10.1128/AEM.01379-19.

Eswayah, A.S., Smith, T.J., Gardiner, P.H.E., 2016. Microbial transformations of selenium species of relevance to bioremediation. Appl. Environ. Microbiol. 82, 4848–4859. https://doi.org/10.1128/AEM.00877-16.

Etteieb, S., Magdouli, S., Zolfaghari, M., Brar, S., 2020. Monitoring and analysis of selenium as an emerging contaminant in mining industry: a critical review. Sci. Total Environ. 698, 134339 https://doi.org/10.1016/j.scitotenv.2019.134339.

Filip'echeva, Y.A., Shelud'ko, A.V., Prilipov, A.G., Burygin, G.L., Telesheva, E.M., Yevstigneyeva, S.S., Chernyshova, M.P., Petrova, L.P., Katsy, E.I., 2018. Plasmid AZOBR_p1-borne *fabG* gene for putative 3-oxoacyl-[acyl-carrier protein] reductase is essential for proper assembly and work of the dual flagellar system in the alphaproteobacterium *Azospirillum brasilense* Sp245. Can. J. Microbiol. 64, 107–118. https://doi.org/10.1139/cjm-2017-0561.

Fischer, S., Krause, T., Lederer, F., Merroun, M.L., Shevchenko, A., Hübner, R., Firkala, T., Stumpf, T., Jordan, N., Jain, R., 2020. *Bacillus safensis* JG-B5T affects the fate of selenium by extracellular production of colloidally less stable selenium nanoparticles. J. Hazard. Mater. 384, 121146 https://doi.org/10.1016/j.jhazmat.2019.121146.

Gómez-Gómez, B., Pérez-Corona, T., Mozzi, F., Pescuma, M., Madrid, Y., 2019. Silac-based quantitative proteomic analysis of *Lactobacillus reuteri* CRL 1101 response to the presence of selenite and selenium nanoparticles. J. Proteom. 195, 53–65. https://doi.org/10.1016/j.jprot.2018.12.025.

Gonzalez-Gil, G., Lens, P.N.L., Saikaly, P.E., 2016. Selenite reduction by anaerobic microbial aggregates: microbial community structure, and proteins associated to the produced selenium spheres. Front. Microbiol. 7, 1–14. https://doi.org/10.3389/fmicb.2016.00571.

Gouveia, D., Grenga, L., Pible, O., Armengaud, J., 2020. Quick microbial molecular phenotyping by differential shotgun proteomics. Environ. Microbiol. 22, 2996–3004. https://doi.org/10.1111/1462-2920.14975.

Hancock, V., Vejborg, R.M., Klemm, P., 2010. Functional genomics of probiotic *Escherichia coli* Nissle 1917 and 83972, and UPEC strain CFT073: comparison of transcriptomes, growth and biofilm formation. Mol. Genet. Genom. 284, 437–454. https://doi.org/10.1007/s00438-010-0578-8.

Harrison, G., Curle, C., Laishley, E.J., 1984. Purification and characterization of an inducible dissimilatory type sulfite reductase from *Clostridium pasteurianum*. Arch. Microbiol. 138, 72–78. https://doi.org/10.1007/BF00425411.

Hayashi, K., Nakashima, R., Sakurai, K., Kitagawa, K., Yamasaki, S., Nishino, K., Yamaguchi, A., 2015. AcrB-AcrA fusion proteins that act as multidrug efflux transporters. J. Bacteriol. 198, 332–342. https://doi.org/10.1128/JB.00587-15.

Hayoun, K., Gouveia, D., Grenga, L., Pible, O., Armengaud, J., Alpha-Bazin, B., 2019. Evaluation of sample preparation methods for fast proteotyping of microorganisms by tandem mass spectrometry. Front. Microbiol. 10, 1985. https://doi.org/10.3389/fmicb.2019.01985.

Hervás, M., López-Maury, L., León, P., Sánchez-Riego, A.M., Florencio, F.J., Navarro, J. A., 2012. ArsH from the cyanobacterium *Synechocystis* sp. PCC 6803 is an efficient NADPH-dependent quinone reductase. Biochemistry 51, 1178–1187. https://doi.org/10.1021/bi201904p.

Huang, Y.-W., Liou, R.-S., Lin, Y.-T., Huang, H.-H., Yang, T.-C., 2014. A linkage between SmeIJK efflux pump, cell envelope integrity, and σ^E-mediated envelope stress response in *Stenotrophomonas maltophilia*. PLoS One 9, e111784. https://doi.org/10.1371/journal.pone.0111784.

Hunter, W.J., 2014a. *Pseudomonas seleniipraecipitans* proteins potentially involved in selenite reduction. Curr. Microbiol. 69, 69–74. https://doi.org/10.1007/s00284-014-0555-2.

Hunter, W.J., 2014b. A *Rhizobium selenitireducens* Protein Showing Selenite Reductase Activity 68, 311–316. ⟨https://doi.org/10.1007/s00284–013-0474–7⟩.

Ibrahim, M., Shi, Y., Qiu, H., Li, B., Jabeen, A., Li, L., Liu, H., Kube, M., Xie, G., Wang, Y., Sun, G., 2012. Differential expression of in vivo and in vitro protein profile of outer membrane of *Acidovorax avenae* subsp. avenae. PLoS One 7, e49657. https://doi.org/10.1371/journal.pone.0049657.

Jahan, Mst I., Juengwiwattanakitti, P., Izu, Y., Tobe, R., Imai, T., Mihara, H., 2019. Selenite uptake by outer membrane porin ExtI and its involvement in the subcellular localization of rhodanese-like lipoprotein ExtH in *Geobacter sulfurreducens*. Biochem. Biophys. Res. Commun. 516, 474–479. https://doi.org/10.1016/j.bbrc.2019.06.037.

Jain, R., Jordan, N., Tsushima, S., Hübner, R., Weiss, S., Lens, P.N.L., 2017. Shape change of biogenic elemental selenium nanomaterials from nanospheres to nanorods decreases their colloidal stability. Environ. Sci. Nano 4, 1054–1063. https://doi.org/10.1039/C7EN00145B.

Kessi, J., 2006. Enzymic systems proposed to be involved in the dissimilatory reduction of selenite in the purple non-sulfur bacteria *Rhodospirillum rubrum* and *Rhodobacter capsulatus*. Microbiology 152, 731–743. https://doi.org/10.1099/mic.0.28240-0.

Khoei, N.S., Lampis, S., Zonaro, E., Yrjälä, K., Bernardi, P., Vallini, G., 2017. Insights into selenite reduction and biogenesis of elemental selenium nanoparticles by two environmental isolates of *Burkholderia fungorum*. New Biotechnol. 34, 1–11. https://doi.org/10.1016/j.nbt.2016.10.002.

Kolodkin-Gal, I., Verdiger, R., Shlosberg-Fedida, A., Engelberg-Kulka, H., 2009. A differential effect of *E. coli* toxin-antitoxin systems on cell death in liquid media and biofilm formation. PLoS One 4, e6785. https://doi.org/10.1371/journal.pone.0006785.

Lampis, S., Zonaro, E., Bertolini, C., Cecconi, D., Monti, F., Micaroni, M., Turner, R.J., Butler, C.S., Vallini, G., 2017. Selenite biotransformation and detoxification by *Stenotrophomonas maltophilia* SeITE02: Novel clues on the route to bacterial biogenesis of selenium nanoparticles. J. Hazard. Mater. 324, 3–14. https://doi.org/10.1016/j.jhazmat.2016.02.035.

Li, D.-B., Cheng, Y.Y., Wu, C., Li, W.W., Li, N., Yang, Z.C., Tong, Z.H., Yu, H.-Q., 2014. Selenite reduction by *Shewanella oneidensis* MR-1 is mediated by fumarate reductase in periplasm. Sci. Rep. 4. https://doi.org/10.1038/srep03735.

Marquez, B., 2005. Bacterial efflux systems and efflux pumps inhibitors. Biochimie 87, 1137–1147. https://doi.org/10.1016/j.biochi.2005.04.012.

McBroom, A.J., Kuehn, M.J., 2007. Release of outer membrane vesicles by Gram-negative bacteria is a novel envelope stress response. Mol. Microbiol. 63, 545–558. https://doi.org/10.1111/j.1365-2958.2006.05522.x.

Merroun, M.L., Raff, J., Rossberg, A., Hennig, C., Reich, T., Selenska-Pobell, S., 2005. Complexation of uranium by cells and S-layer sheets of *Bacillus sphaericus* JG-A12. Appl. Environ. Microbiol. 71, 5532–5543. https://doi.org/10.1128/AEM.71.9.5532-5543.2005.

Nancharaiah, Y.V., Lens, P.N.L., 2015. Selenium biomineralization for biotechnological applications. Trends Biotechnol. 33, 323–330. https://doi.org/10.1016/j.tibtech.2015.03.004.

Ni, T.W., Staicu, L.C., Nemeth, R.S., Schwartz, C.L., Crawford, D., Seligman, J.D., Hunter, W.J., Pilon-Smits, E.A.H., Ackerson, C.J., 2015. Progress toward clonable inorganic nanoparticles. Nanoscale 7, 17320–17327. https://doi.org/10.1039/C5NR04097C.

Noinaj, N., Guillier, M., Barnard, T.J., Buchanan, S.K., 2010. TonB-dependent transporters: regulation, structure, and function. Annu. Rev. Microbiol. 64, 43–60. https://doi.org/10.1146/annurev.micro.112408.134247.

Perez-Riverol, Y., Zorin, A., Dass, G., Vu, M.-T., Xu, P., Glont, M., Vizcaíno, J.A., Jarnuczak, A.F., Petryszak, R., Ping, P., Hermjakob, H., 2019. Quantifying the impact of public omics data. Nat. Commun. 10, 3512. https://doi.org/10.1038/s41467-019-11461-w.

Pinel-Cabello, M., Jroundi, F., López-Fernández, M., Geffers, R., Jarek, M., Jauregui, R., Link, A., Vílchez-Vargas, R., Merroun, M.L., 2021. Multisystem combined uranium resistance mechanisms and bioremediation potential of *Stenotrophomonas bentonitica* BII-R7: transcriptomics and microscopic study. J. Hazard. Mater. 403, 123858 https://doi.org/10.1016/j.jhazmat.2020.123858.

Poirier, I., Kuhn, L., Demortière, A., Mirvaux, B., Hammann, P., Chicher, J., Caplat, C., Pallud, M., Bertrand, M., 2016. Ability of the marine bacterium *Pseudomonas fluorescens* BA3SM1 to counteract the toxicity of CdSe nanoparticles. J. Proteom. 148, 213–227. https://doi.org/10.1016/j.jprot.2016.07.021.

Presentato, A., Piacenza, E., Anikovskiy, M., Cappelletti, M., Zannoni, D., Turner, R.J., 2018. Biosynthesis of selenium-nanoparticles and -nanorods as a product of selenite bioconversion by the aerobic bacterium *Rhodococcus aetherivorans* BCP1. New Biotechnol. 41, 1–8. https://doi.org/10.1016/j.nbt.2017.11.002.

Ranjard, L., Prigent-Combaret, C., Nazaret, S., Cournoyer, B., 2002. Methylation of inorganic and organic selenium by the bacterial thiopurine methyltransferase. J. Bacteriol. 184, 3146–3149. https://doi.org/10.1128/JB.184.11.3146-3149.2002.

Rayman, M.P., 2012. Selenium and human health. Lancet 379, 1256–1268. https://doi.org/10.1016/S0140-6736(11)61452-9.

Rosenfeld, C.E., Kenyon, J.A., James, B.R., Santelli, C.M., 2017. Selenium (IV,VI) reduction and tolerance by fungi in an oxic environment. Geobiology 15, 441–452. https://doi.org/10.1111/gbi.12224.

Ruiz Fresneda, M.A., Delgado Martín, J., Gómez Bolívar, J., Fernández Cantos, M.V., Bosch-Estévez, G., Martínez Moreno, M.F., Merroun, M.L., 2018. Green synthesis and biotransformation of amorphous Se nanospheres to trigonal 1D Se nanostructures: impact on Se mobility within the concept of radioactive waste disposal. Environ. Sci. Nano 5, 2103–2116. https://doi.org/10.1039/C8EN00221E.

Ruiz-Fresneda, M.A., Eswayah, A.S., Romero-González, M., Gardiner, P.H.E., Solari, P.L., Merroun, M.L., 2020. Chemical and structural characterization of Se^{IV} biotransformations by *Stenotrophomonas bentonitica* into Se^0 nanostructures and volatiles Se species. Environ. Sci. Nano 7, 2140–2155. https://doi.org/10.1039/D0EN00507J.

Ruiz-Fresneda, M.A., Gomez-Bolivar, J., Delgado-Martin, J., Abad-Ortega, M., del, M., Guerra-Tschuschke, I., Merroun, M.L., 2019. The bioreduction of selenite under anaerobic and alkaline conditions analogous to those expected for a deep geological repository system. Molecules 24, 3868. https://doi.org/10.3390/molecules24213868.

Sánchez-Castro, I., Bakkali, M., Merroun, M.L., 2017. Draft genome sequence of *Stenotrophomonas bentonitica* BII-$R7^T$, a selenite-reducing bacterium isolated from Spanish bentonites. Genome Announc. 5. https://doi.org/10.1128/genomeA.00719-17.

Schilling, K., Basu, A., Wanner, C., Sanford, R.A., Pallud, C., Johnson, T.M., Mason, P.R. D., 2020. Mass-dependent selenium isotopic fractionation during microbial reduction of seleno-oxyanions by phylogenetically diverse bacteria. Geochim. Cosmochim. Acta 276, 274–288. https://doi.org/10.1016/j.gca.2020.02.036.

Srivastava, N., Mukhopadhyay, M., 2015. Green synthesis and structural characterization of selenium nanoparticles and assessment of their antimicrobial property. Bioprocess Biosyst. Eng. 38, 1723–1730. https://doi.org/10.1007/s00449-015-1413-8.

Taylor, J.A., Bratton, B.P., Sichel, S.R., Blair, K.M., Jacobs, H.M., DeMeester, K.E., Kuru, E., Gray, J., Biboy, J., VanNieuwenhze, M.S., Vollmer, W., Grimes, C.L., Shaevitz, J.W., Salama, N.R., 2020. Distinct cytoskeletal proteins define zones of enhanced cell wall synthesis in *Helicobacter pylori*. eLife 9, e52482. https://doi.org/10.7554/eLife.52482.

Vorontsov, I.I., Minasov, G., Brunzelle, J.S., Shuvalova, L., Kiryukhina, O., Collart, F.R., Anderson, W.F., 2007. Crystal structure of an apo form of *Shigella flexneri* ArsH protein with an NADPH-dependent FMN reductase activity. Protein Sci. 16, 2483–2490. https://doi.org/10.1110/ps.073029607.

Wadhwani, S.A., Shedbalkar, U.U., Singh, R., Chopade, B.A., 2018. Biosynthesis of gold and selenium nanoparticles by purified protein from *Acinetobacter* sp. SW 30. Enzym. Microb. Technol. 111, 81–86. https://doi.org/10.1016/j.enzmictec.2017.10.007.

Wang, Y., Shu, X., Hou, J., Lu, W., Zhao, W., Huang, S., Wu, L., 2018. Selenium Nanoparticle Synthesized by *Proteus mirabilis* YC801: an efficacious pathway for selenite biotransformation and detoxification. Int. J. Mol. Sci. 19, 3809. https://doi.org/10.3390/ijms19123809.

Wang, T., Yang, L., Zhang, B., Liu, J., 2010. Extracellular biosynthesis and transformation of selenium nanoparticles and application in H_2O_2 biosensor. Colloids Surf. B Biointerfaces 80, 94–102. https://doi.org/10.1016/j.colsurfb.2010.05.041.

Wells, M., McGarry, J., Gaye, M.M., Basu, P., Oremland, R.S., Stolz, J.F., 2019. Respiratory selenite reductase from *Bacillus selenitireducens* strain MLS10. J. Bacteriol. 201, e00614-18 https://doi.org/10.1128/JB.00614-18.

Winkel, L.H.E., Vriens, B., Jones, G.D., Schneider, L.S., Pilon-Smits, E., Bañuelos, G.S., 2015. Selenium cycling across soil-plant-atmosphere interfaces: a critical review. Nutrients 7, 4199–4239. https://doi.org/10.3390/nu7064199.

Xu, D., Yang, L., Wang, Y., Wang, G., Rensing, C., Zheng, S., 2018. Proteins enriched in charged amino acids control the formation and stabilization of selenium nanoparticles in *Comamonas testosteroni* S44. Sci. Rep. 8, 4766. https://doi.org/10.1038/s41598-018-23295-5.

Zhang, J., Wang, Y., Shao, Z., Li, J., Zan, S., Zhou, S., Yang, R., 2019. Two selenium tolerant *Lysinibacillus* sp. strains are capable of reducing selenite to elemental Se efficiently under aerobic conditions. J. Environ. Sci. 77, 238–249. https://doi.org/10.1016/j.jes.2018.08.002.